Chapter 18
The Geos-Chem Model

Lyatt Jaeglé, Sarah A. Strode, Noelle E. Selin, and Daniel J. Jacob

Summary We examine the response of deposition to decreases in anthropogenic emissions using the GEOS-Chem global atmosphere-ocean-land mercury simulation. Total global mercury sources in the model are 9230 Mg yr^{-1} (3400 Mg yr^{-1} anthropogenic, 650 Mg yr^{-1} biomass burning, 2180 Mg yr^{-1} land emissions, 3000 Mg yr^{-1} ocean emissions). Our atmospheric simulation describes the cycling of mercury through the surface ocean and land reservoirs. The model includes atmospheric oxidation of Hg^0 by OH and O_3, and in-cloud reduction of $Hg^{(II)}$. Wet and dry deposition account for 32% and 68% of the global sink, respectively. The lifetime of mercury against deposition is 0.6 years. We conduct four sensitivity simulations where anthropogenic emissions are reduced by 20% over East Asia, Europe, South Asia, and North America, leading to decreases in global deposition of -3.5, -0.9, -0.8, and -0.5% respectively. One third of the deposition decrease occurs in the source regions, and the rest is distributed globally due to decreased long-range transport of Hg^0 and subsequent oxidation to $Hg^{(II)}$. Regional decreases in deposition within the source regions range from -12% for East Asia (60% of depositions due to local emissions) to -3% for North America (where only 15% of deposition is due to local emissions). When normalized by total emissions, we find that Hg deposition in the Arctic is more sensitive to decreases in European emissions compared to decreases in East Asian, North American, or South Asian emissions. Our estimates of the distribution of deposition and its response to decreases in anthropogenic emissions are limited by uncertainties in the speciation of anthropogenic emissions, redox chemistry of atmospheric mercury, the role of dry deposition, and the cycling efficiency of mercury in the ocean and land reservoirs.

18.1 Introduction

The dual character of mercury as a local and global pollutant makes it difficult to assess the relative contributions of regional and global sources to deposition. Anthropogenic emissions of mercury as short-lived reactive gaseous ($Hg^{(II)}$) and particulate (Hg(p)) mercury forms lead to rapid deposition near source regions.

N. Pirrone and R. Mason (eds.), *Mercury Fate and Transport in the Global Atmosphere*,
DOI: 10.1007/978-0-387-93958-2_18,

If mercury is emitted in its long-lived elemental form (Hg^0), it can be transported on global scales, oxidized to $Hg^{(II)}$, and then deposited far from source regions. In addition, dry deposition of Hg^0 itself can affect receptor regions. Cycling of anthropogenic mercury through land and ocean surfaces further complicates source attribution of mercury.

In this chapter, we use the GEOS-Chem global mercury simulation to examine the response of deposition to decreased anthropogenic emissions for four regions in the Northern Hemisphere. We examine source-receptor relationships from regional to global scales, and assess the role of cycling of anthropogenic mercury in the surface ocean and land reservoirs.

18.2 Model Description

The GEOS-Chem chemical transport model (Bey et al., 2001) simulates mercury in the atmosphere-ocean-land system. We use here model version 7.04 (http://www.harvard.as.edu/chemistry/trop/geos). The atmospheric mercury simulation is described in Selin et al. (2007) and has a horizontal resolution of 4 degrees latitude by 5 degrees longitude and 30 vertical levels. It is driven by assimilated meteorological observations from the NASA Goddard Earth Observing System (GEOS-4). Three atmospheric mercury species are simulated: elemental mercury (Hg^0), oxidized mercury ($Hg^{(II)}$), and refractory particulate mercury (Hg(p)).

Emissions are shown in Table 18.1 and Figure 18.1 and described in Selin et al. (2007). Anthropogenic emissions are based on the Pacyna et al. (2006) inventory for year 2000, with updates described in Selin et al. (2008): 50% increase in Asia, consistent with estimates of Jaffe et al. (2005) and Strode et al. (2008), and a 30%

Table 18.1 Budget of mercury in the GEOS-Chem model for the globe and the four HTAP regions

	Global	East Asia	Europe	South Asia	N. America
Total Sources ($Mg\ yr^{-1}$)	9230	1980	720	680	780
Anthropogenic	3400	1340	380	300	190
Biomass Burning	650	70	10	70	30
Land[1]	1700	290	230	110	320
Prompt Land recycling	480	80	60	60	50
Ocean[2]	3000	200	40	140	190
Total Sinks ($Mg\ yr^{-1}$)	9230	1080	560	630	900
Dry Deposition[3]	6300	750	470	410	590
Wet Deposition	2930	340	90	220	310
Mercury burden (Mg)	5600				
Mercury burden (yr)	0.6				

[1] The land source includes geogenic, evapotranspiration, and soil emissions.

[2] The ocean source listed in the table is the net ocean evasion via gas exchange.

[3] Dry deposition does not include the dry deposition of Hg^0 over the ocean, which is treated as part of the ocean term.

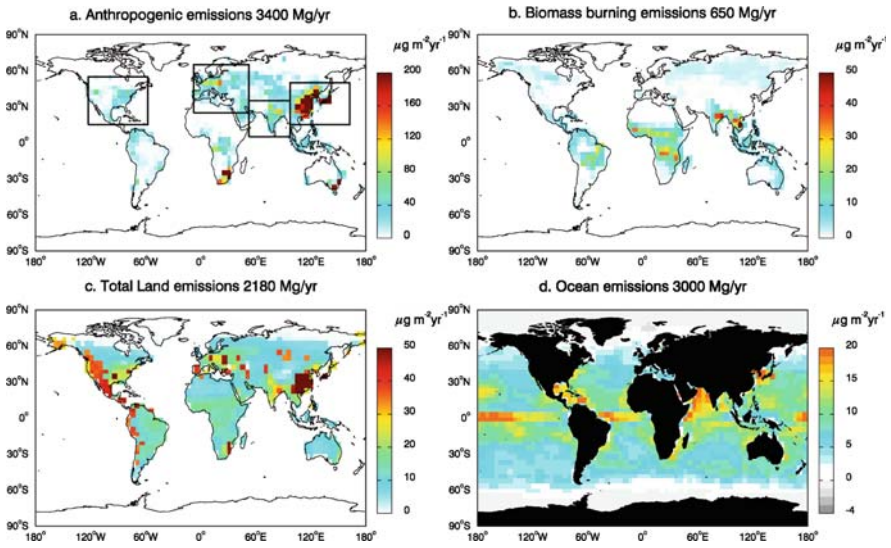

Figure 18.1 Global distribution of annual emissions ($\mu g\, m^{-2} yr^{-1}$) in the GEOS-Chem model: A) Anthropogenic, B) biomass burning, C) land, and D) ocean emissions. The domains for the four HTAP regions are indicated on panel a)

increase in the rest of the world in order to obtain an unbiased simulation. These modifications add 760 Mg yr^{-1} to the 2190 Mg yr^{-1} Pacyna et al., (2006) inventory. Our inventory also includes a 450 Mg yr^{-1} source of Hg^0 from artisanal mining, resulting in global anthropogenic emissions of 3400 Mg yr^{-1} (2215 Mg yr^{-1} Hg^0, 935 Mg yr^{-1} $Hg^{(II)}$, and 250 Mg yr^{-1} Hg(p)). Biomass burning emissions account for 650 Mg yr^{-1}, and are based on a monthly climatological biomass burning CO inventory (Duncan et al., 2003) scaled with a 2.1×10^{-7} Hg^0/CO emission ratio.

The atmospheric model is fully coupled with a mixed-layer slab ocean model described in Strode et al. (2007). The ocean model includes interactions of the mixed layer with the atmosphere and deep ocean, as well as conversion of among elemental, divalent, and nonreactive aqueous mercury species. The model is constrained to reproduce mean observed aqueous concentrations. We find a net Hg^0 global net ocean evasion flux of 3000 Mg yr^{-1} Hg^0. Re-emission of previously deposited mercury accounts for 89% of our ocean emissions, with the remaining fraction coming from upwelling of mercury from below the mixed layer.

The atmospheric model is fully coupled with a mixed-layer slab ocean model described in Strode et al. (2007). The ocean model includes interactions of the mixed layer with the atmosphere and deep ocean, as well as conversion of among elemental, divalent, and nonreactive aqueous mercury species. The model is constrained to reproduce mean observed aqueous concentrations. We find a net Hg^0 global net ocean evasion flux of 3000 Mg yr^{-1} Hg^0. Re-emission of previously

deposited mercury accounts for 89% of our ocean emissions, with the remaining fraction coming from upwelling of mercury from below the mixed layer.

Land-atmosphere exchange of mercury is mechanistically parameterised, resulting in a net Hg^0 land source of 2180 Mg yr^{-1} (Selin et al., 2008). Land emissions include soil volatilisation, evapotranspiration, and a geogenic source, which together account for 1700 Mg yr^{-1}. In addition, the land source includes partial recycling of recently deposited mercury (480 Mg yr^{-1}). For this recycling component, we assume that 20% of $Hg^{(II)}$ and Hg(p) deposited to land immediately returns to the atmosphere as Hg^0 (this number is increased to 60% for snow-covered surfaces).

In the atmosphere Hg^0 is oxidized by OH and O_3, while in clouds $Hg^{(II)}$ is photochemically reduced to Hg^0. $Hg^{(II)}$ and Hg(p) are removed by wet deposition, with Hg(p) scavenged as a water soluble aerosol, and $Hg^{(II)}$ scavenged as a highly water soluble gas (Selin et al., 2007). Dry deposition to land of all three species is based on a resistance in series scheme. The model also includes dry deposition of $Hg^{(II)}$ over the oceans by loss on sea-salt aerosols. Dry deposition of Hg^0 to the ocean is included in the gas exchange ocean parameterisation.

In the simulations presented here, we use meteorological observations for the year 2001, with a 5-year spin-up period (repeating the year 2001) for the reference simulation. In addition, we conduct four perturbation experiments where primary anthropogenic emissions are reduced by 20% for each of the following regions: East Asia (EA: 15-50º N; 95-160º E), Europe and North Africa (EU: 25-65º N; 10º W-50º E), South Asia (SA: 5-35º N; 50-95º E), and North America (NA: 15-55º N; 125-60º W). The definition of these regions follows the guidelines of the Task Force on Hemispheric Transport of Air Pollution (TF HTAP) perturbation experiments (http://aqm.jrc.it/HTAP/). For each 20% perturbation experiment, we run the model for 5 additional years and present the results for the last year.

18.3 Results/Discussion

In this section, we briefly present results from our reference simulation (section 18.3.1), and then discuss the results of the perturbation experiments, focusing on the response of Hg deposition rates to emission reductions (section 18.3.2) and on the effects on land and ocean cycling (section 18.3.3).

18.3.1 Reference Simulation

Annual mean distributions of surface concentrations of Hg^0 and $Hg^{(II)}$ + Hg(p) are presented in Figure 18.2 (top panels). In the model, globally averaged surface concentrations of total mercury are 1.5 ng m^{-3}, with $Hg^{(II)}$ + Hg(p) accounting for 0.03 ng m^{-3}. Enhanced concentrations of Hg^0 are found over industrial regions, reaching

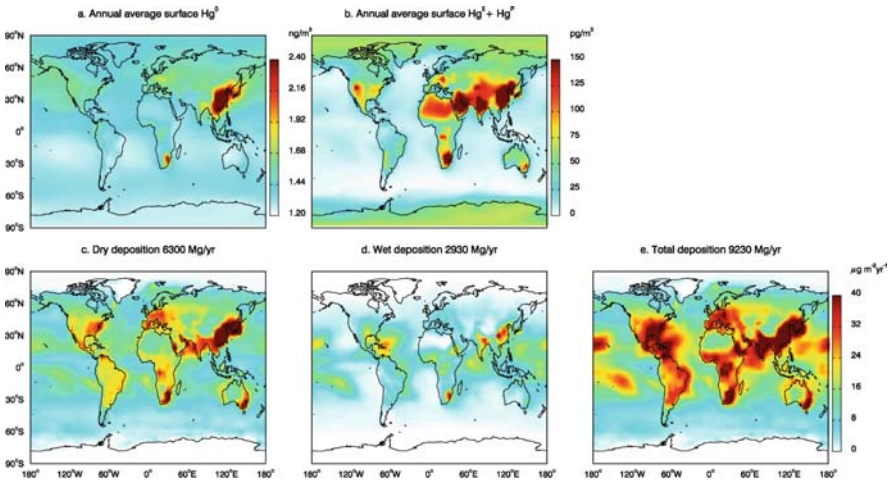

Figure 18.2 Annual mean distribution of surface concentrations of a) Hg^0(*ng m*$^{-3}$) and b) $Hg^{(II)}$ + Hg(p) (*pg m*$^{-3}$). The bottom three figures show the annual mean distribution of deposition fluxes ($\mu g\ m^{-2}yr^{-1}$): c) Dry deposition, d) Wet deposition, and e) Total deposition

>2.4 ng m^{-3} over East Asia (Figure 18.2), which accounts for 39% of global anthropogenic emissions (see Table 18.1). $Hg^{(II)}$ and Hg(p) are emitted by anthropogenic sources and elevated concentrations are generally located over industrial regions. Elevated $Hg^{(II)}$ levels also occur over mountains and deserts, where enhanced mixing of free tropospheric air brings down high $Hg^{(II)}$. Over deserts, weak wet deposition of $Hg^{(II)}$ further contributes to the enhancement. Concentrations of $Hg^{(II)}$ increase with altitude in the model because of the source from oxidation of the global Hg^0 pool and longer lifetime of $Hg^{(II)}$, consistent with observations (Swartzendruber et al., 2006). Low $Hg^{(II)}$ concentrations occur over oceans, where loss on sea-salt aerosols dominates dry deposition.

Selin et al. (2007) have conducted detailed comparisons of the model to surface observations of Hg^0, $Hg^{(II)}$, and Hg(p) and find reasonable agreement. The model reproduces mean annual concentrations total gaseous mercury (TGM = Hg^0 + $Hg^{(II)}$) concentrations at land sites, but underestimates cruise observations in the North Atlantic and North Pacific by 25%. The model interhemispheric gradient for TGM is 1.2, consistent with land-based observations, but lower than the 1.5 gradient inferred from cruise observations. The reason for the discrepancy is unclear. The model captures the observed seasonal cycle of TGM at surface sites in the northern hemisphere.

Globally, wet deposition results in a 2930 Mg yr^{-1} sink of mercury (93% as $Hg^{(II)}$ and the rest as Hg(p)), while dry deposition yields a 6300 Mg yr^{-1} sink (26% Hg^0, 73% $Hg^{(II)}$, 1% Hg(p)). The overall lifetime of mercury in the model against deposition is 0.6 years (Table 18.1). The spatial distribution of deposition is shown on the bottom panels of Figure 18.2. The model reproduces the observed spatial and temporal distribution of wet deposition over the U.S. (Selin and Jacob, 2008).

18.3.2 Response of Deposition to Anthropogenic Emission Reductions

Together, the four regions where the perturbation experiments are conducted comprise 65% of global anthropogenic emissions, with EA alone accounting for 39% (1340 Mg yr^{-1}) of global anthropogenic emissions, while NA accounts for only 6% (190 Mg yr^{-1}) (Table 18.1).

Table 18.2 summarizes the global annual changes in emissions and deposition for the 20% anthropogenic perturbation experiments. The magnitude of the decrease in global deposition is proportional to the magnitude of the initial reduction in anthropogenic sources. Thus EA has the largest effect both globally and locally, and NA has the smallest effect. We find that the decrease in global deposition is 25-30% larger than the initial decrease in anthropogenic emissions. This amplification is due to response of the surface land and ocean reservoirs, and is discussed in more detail in section 3.3.

Table 18.3 summarizes the absolute changes in deposition over land for each pair of source-receptors and for the globe. For a given region, Hg deposition is due

Table 18.2 Global annual change in sources and sinks for the four perturbation simulations

	ΔEast Asia	ΔEurope	ΔSouth Asia	ΔNorth America
Change in emissions (*Mg yr*$^{-1}$)	-326	-85.4	-71.8	-46.6
Anthropogenic (-20%)	-262	-69	-56.5	-37.3
Land[1]	-20	-6.9	-5.2	-3.7
Ocean[1]	-44	-9.5	-10.1	-5.6
Change in deposition (*Mg yr*$^{-1}$)	-323	-84.7	-71.3	-46.2
Dry Deposition	-220	-59.5	-45.8	-30.5
Wet Deposition	-103	-25.2	-25.5	-15.7
Amplification factor $\frac{\Delta Deposition}{\Delta Anthropogenic}$	1.23	1.23	1.26	1.24

[1]The change in ocean and land emissions is calculated interactively in response to the 20% reduction in anthropogenic emissions for each region.

[2]The last row shows the amplification factor, which we define as the change in deposition divided by the change in anthropogenic emissions.

Table 18.3 Absolute change (in *Mg* yr^{-1}) in deposition over land for each pair of source-receptor regions and for the globe.

Receptors Sources	EastAsia	Europe	South Asia	N. America	Global (land only)	Global (all)
East Asia	-76	-13	-9.9	-15	-167	-323
Europe	-2.7	-23	-3.3	-3.6	-48	-85
South Asia	-2.4	-3.4	-18	-2.6	-36	-71
North America	-1.1	-2.1	-1.2	-14	-25	-46

Each line corresponds to the results of a perturbation experiment, while the columns show the response in the receptor regions. The last 2 columns show the global decrease in deposition over land only and everywhere.

to a combination of deposition of local anthropogenic emissions of $Hg^{(II)}$ and HgP and of oxidation of the global Hg^0 pool to $Hg^{(II)}$. Because of their short lifetimes, most of the anthropogenic $Hg^{(II)}$ and Hg(p) emissions are deposited near sources, while the anthropogenic Hg^0 can be transported globally and contribute to the global Hg^0 pool.

Overall, we find that 24-31% of the total change in deposition occurs over the land in the source regions (Table 18.3), another 5-10% occurs over the oceans in source regions. The remaining change in deposition is distributed globally as a result of the decrease in the global Hg^0 pool.

Figure 18.3 show the global distribution in the deposition decrease (in percent) for each perturbation experiment relative to the reference simulation, while Figure 18.4 zooms in on the deposition decrease over emission regions.

The percentage decreases in deposition over land are also summarized in Table 18.4. This percentage decrease in deposition over source regions reflects the relative contribution from local anthropogenic Hg emissions and from the global Hg^0 pool. Thus, if local deposition were solely controlled by anthropogenic emissions within the region, we would expect a 20% decrease in anthropogenic emissions to result in a 20% decrease in deposition in that region. Instead, we find decreases ranging from -12% to -3%. The EA region displays the largest reduction in local deposition

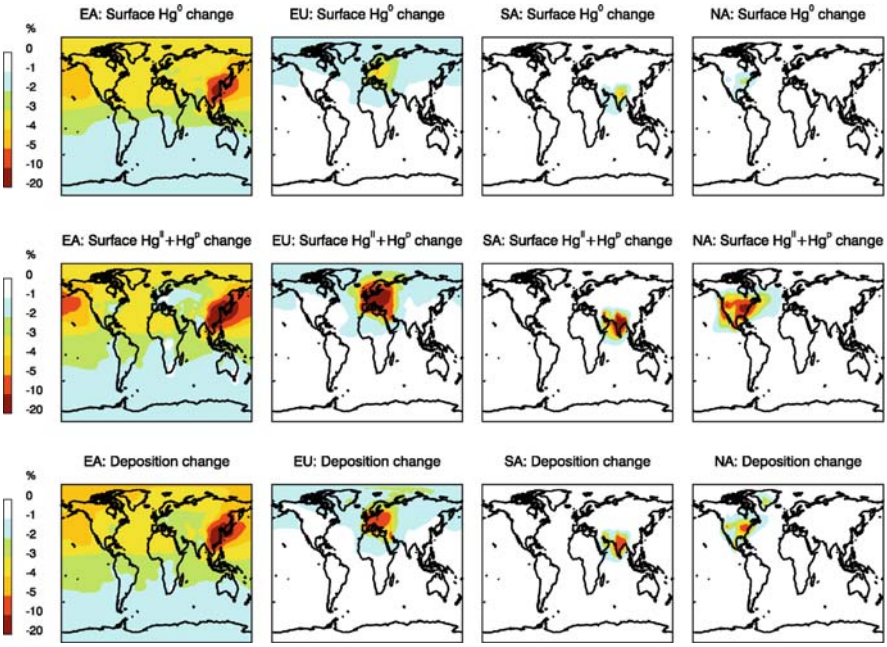

Figure 18.3 Percentage change in annual surface concentrations of Hg^0 and $Hg^{(II)}$ + Hg(p) (top 2 rows) and in deposition (bottom row) for each perturbation simulation. The perturbation simulations are shown from left to right: East Asia (EA), Europe and North Africa (EU), South Asia (SA), and North America (NA)

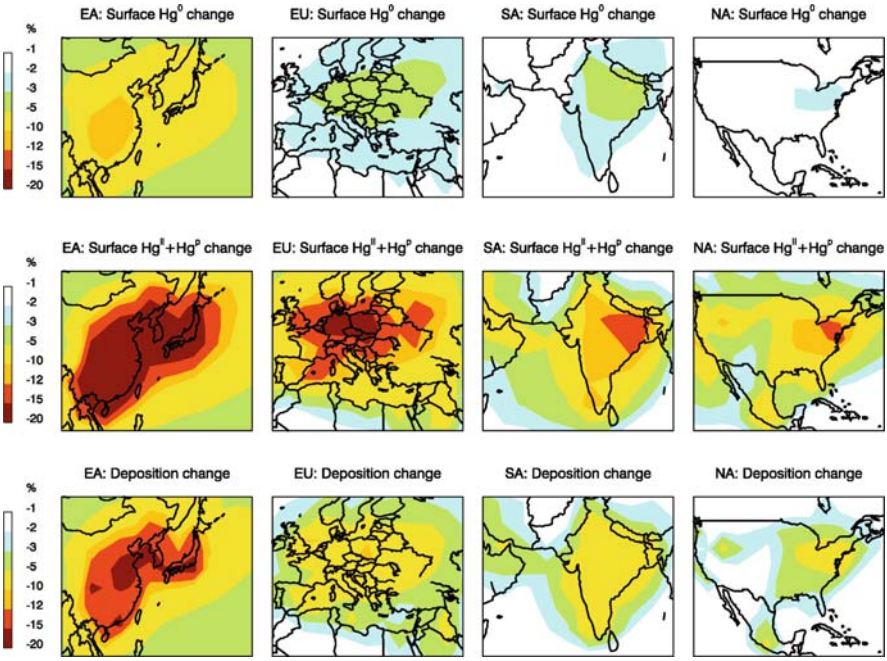

Figure 18.4 Same as Figure 18.3, but focusing on the source regions where anthropogenic emissions are reduced by 20%

Table 18.4 Mean relative change (%) in deposition over land for each pair of source-receptor regions and for the globe

Receptor: Source:	East Asia	Europe	South Asia	N.America	Global (land only)	Global (all)
East Asia	-12.3	-2.8	-2.7	-3.2	-4.0	-3.5
Europe	-0.43	-4.7	-0.88	-0.76	-1.2	-0.9
South Asia	-0.39	-0.7	-4.8	-0.55	-0.9	-0.8
North America	-0.18	-0.44	-0.33	-3.0	-0.6	-0.5

Table 18.5 Relative change in Hg^0, and $Hg^{(II)}$ + Hg(p) concentrations (%) for each pair of source-receptor region

Receptor: Source:	East Asia	Europe	South Asia	N. America	Global
East Asia	-7.6, -14	-3.2, -2.2	-3.1, -2.4	-3.5, -2.8	-3.1, -3.6
Europe	-0.8, -0.4	-2.5, -7.3	-0.9, -1	-0.9, -0.7	-1, -1.4
South Asia	-0.5, -0.3	-0.6, -0.9	-2.1, -6.5	-0.5, -0.5	-0.6, -0.9
North America	-0.3, -0.2	-0.5, -0.3	-0.4, -0.3	-1.1, -5.8	-0.4, -0.6

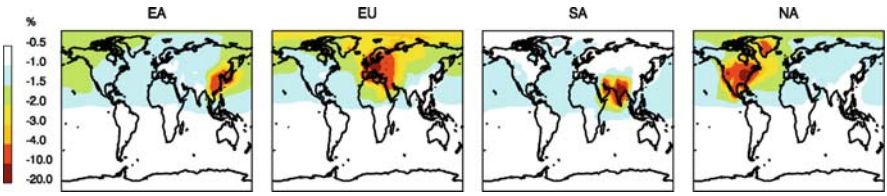

Figure 18.5 Change in annual deposition. Same as bottom panel in Figure 18.3, but scaled to a 100 Mg yr^{-1} anthropogenic emission decrease for each region

(-12%), this implies that about 60% (obtained by dividing 12 by 20) of the deposition in EA is the result of local emissions. In contrast, for NA we only find a 3% decrease in deposition, thus about 15% of the deposition in that region is due to NA anthropogenic emissions. The rest comes from oxidation of the global Hg^0 pool. This is consistent with Selin and Jacob (2008), who found that a significant fraction of wet deposition over NA results from scavenging of $Hg^{(II)}$ in the free troposphere above 850 hPa. For the EU and SA regions, we find local decreases in deposition of 5%, implying that regional emissions account for ~25% of local deposition.

Globally averaged, decreases in deposition range from 3.5% for a reduction in EA anthropogenic emissions, to less than 1% for reductions in the NA source (Table 18.4). Regions with low anthropogenic sources are the most affected by outside influence. For example, a 20% reduction in EA emissions leads to a larger decrease in NA (-3.2%) than a 20% reduction in local anthropogenic emissions in NA (-3%).

What is the relative efficiency of different regions in affecting deposition over remote regions? We assess this by normalizing the decreases in deposition to a 100 Mg yr^{-1} decrease in anthropogenic emissions. We thus multiply the deposition decreases from Figure 18.3 by global scaling factors of 0.4, 1.4, 1.8, 2.7 for EA, EU, SA, and NA, respectively. This assumes a linear response of deposition to emission changes (we verified that it is a reasonable assumption by conducting perturbation experiments varying the decrease in emissions). The results are displayed in Figure 18.5.

We see that a region of particular sensitivity to emission reductions is the Arctic (defined here as latitudes poleward of 65 N). Reductions in anthropogenic emissions from EA, EU, SA, EA contributed to deposition decreases in the Arctic of -3.8%, -1.55%, -0.53%, -0.54%, respectively. When we normalize these numbers to 100 Mg/yr decrease in anthropogenic emissions, we obtain -1.4%, -2.2%, -0.9%, -1.4%. We thus find that European emissions lead to a deposition decrease that is 60% larger than either EA or NA. Compared to SA, European emissions are a factor of 2.4 more effective. This is consistent with our general understanding of transport pathways to the Arctic (Stohl et al., 2002; Travnikov, 2005). Thus is would seem that decreases in European mercury emissions will be the most effective on a per Mg basis at reducing Hg contamination in the Arctic. However, anthropogenic European emissions have already been strongly reduced over the past decades, and at present they are three times smaller than emissions from EA. Thus, EA emissions have the strongest influence on current Arctic deposition. Note that

we do not have a representation of fast oxidation of Hg^0 during springtime mercury depletion events. This process is likely to enhance overall deposition, but should not affect the relative efficiency of source regions.

18.3.3 Response of Land and Ocean Emissions

Our coupled land-atmosphere-ocean mercury simulation allows us to examine how reduced anthropogenic emissions affect the rapid cycling of mercury in the land and ocean reservoirs. Atmospheric deposition is the main source of mercury to the surface ocean. Thus, a decrease in deposition of anthropogenic mercury leads to a decrease in the concentrations of mercury in the surface ocean, which in turn results in a decrease in the net ocean-atmosphere flux. Because of the rapid cycling of Hg between the atmosphere and surface ocean, a new steady-state is reached within 2-3 years in our perturbation simulations. Similarly, prompt recycling of land emissions responds rapidly through the recycling of deposited mercury, as we assume steady-state between local deposition and land recycling. Over longer timescales (decades to centuries) exchange of Hg with the thermocline, and land cycling through evapotranspiration and volatilization will also respond, but we do not take these changes into account here.

Table 18.2 summarizes the reduction in land and ocean emissions for each anthropogenic perturbation simulation. We find that the response of these reservoirs leads to a significant amplification of the initial reduction in primary anthropogenic emissions. For example, decreasing East Asian anthropogenic emissions by 20% (-262 Mg yr^{-1}) leads to a 44 Mg yr^{-1} reduction in ocean emissions and a 20 Mg/yr reduction in land emissions. The resulting change in Hg cycling leads to an overall decrease in emissions (and thus deposition) that is 1.25 times larger than the initial change in anthropogenic emissions. Similar amplification factors (1.23-1.26) are found for the other sources regions.

The spatial distribution of the reduction in land and ocean emissions is shown in Figure 18.6. We find that half of the reduction in land emissions occurs within the source region, in response to local decreases in deposition. The remaining 50% occurs outside these source regions, as a result of decreased long-range transport of Hg^0 anthropogenic emissions, conversion to $Hg^{(II)}$, and deposition.

For ocean emissions, we see significant decreases in the coastal regions near sources (N. American East coast, Northwest Pacific, Mediterranean, Indian Sea), but the decreases are distributed more globally, with 75% of the reduced ocean emissions occurring outside the source regions (Figure 18.6). The areas with large decreases are concentrated in the Tropics, where high deposition rates and oceanic biological productivity lead to rapid reduction of deposited aqueous $Hg^{(II)}$ to aqueous Hg^0, which is then released to the atmosphere. At high latitudes, the cold water is undersaturated in Hg^0 and the ocean is a net sink for Hg^0 (Figure 18.1). Thus, as atmospheric Hg^0 decreases in our perturbation experiments, the ocean becomes less undersaturated, leading to a net increase in air-sea exchange in the high-latitude North Atlantic Ocean and Southern Ocean.

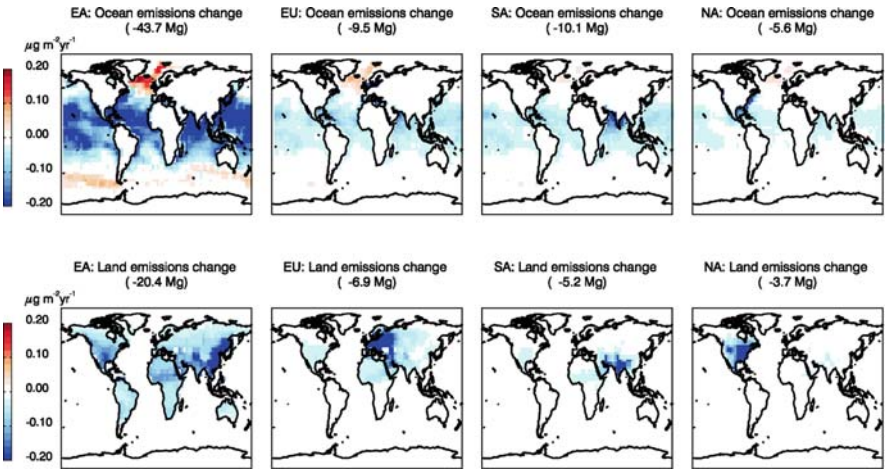

Figure 18.6 Distribution of absolute change ($\mu g\ m^{-2}\ yr^{-1}$) in annual mean ocean (top), and land (bottom) emissions for each perturbation simulation

18.4 Uncertainties in Model Results and Future Research

The distribution of deposition and its response to decreases in anthropogenic emissions is affected by a number of key uncertainties: speciation of anthropogenic emissions, reduction-oxidation chemistry of mercury in the atmosphere and clouds, precipitation, dry deposition, and cycling in land and ocean reservoirs. We briefly discuss each of these uncertainties below and emphasize areas of future research.

The speciation of anthropogenic emissions as $Hg^0/Hg^{(II)}/Hg(p)$ is poorly understood, as few source test measurements exist. In our emission inventory, $Hg^{(II)}$ + Hg(p) account for 35% of global anthropogenic emissions. This number increases to 45% for regions dominated by coal combustion. If a higher fraction of Hg were to be emitted as reactive mercury, this would lead to an increase in local deposition of $Hg^{(II)}$ + Hg(p) and reduced long-range transport of Hg^0. Assumptions about the redox chemistry of Hg in the atmosphere will also affect our results. Our chemistry scheme is very simple compared to other more complex model implementations (Ryaboshapko et al., 2002). Given the poor knowledge of rate constants, our approach has been to only implement two oxidation reactions (O_3 and OH) and adjust the rate of in-cloud photochemical reduction to best reproduce observed global Hg concentrations and seasonal variation at Northern mid-latitudes. Currently, we do not take into account halogen oxidation of Hg^0, which can be significant in polar regions, marine boundary layer, and upper troposphere (Holmes et al., 2006), but we will implement this in the future.

Dry deposition plays a dominant role in our simulated global deposition (Table 18.1). Few measurements of Hg dry deposition velocities exist. Our simulation of a large Hg^0 dry deposition over land and $Hg^{(II)}$ deposition over the oceans by sea-salt uptake, while consistent with the existing few measurements, is thus poorly constrained.

The fraction of newly deposited Hg that is available for cycling back to the atmosphere is assumed to be 20% for land surface, in the mid-range of cycling efficiencies inferred by isotopic observations (Amyot et al., 2004; Hintelmann et al., 2002). This cycling is likely to be a function of vegetation type and soil properties, which would induce variability that is not currently taken into account. Such prompt recycling is a small fraction of the total land source. The remaining, much larger, land sources will also respond to perturbations in deposition, but over a much longer time-scale, introducing a lag-time that is poorly constrained.

For the ocean emissions, we do not take into account horizontal transport of aqueous mercury and neglect riverine input of Hg. Both these factors could affect the spatial distribution of the air-sea flux of Hg^0 and its response to reduced anthropogenic emissions. In addition, exchange of mercury between the thermocline and the surface ocean will result in a response time of decades to centuries.

More generally, an increasing number of global mercury models have been developed over the past 5 years (as can be seen from the chapters in part III of this report), but the observational constraints on these models remain limited. In particular very few measurements of speciated mercury in the free troposphere exist. Such measurements, conducted on aircraft over continental scales would help quantify the distribution and chemical transformation of mercury in the free troposphere and provide crucial validation for global and regional models.

References

Amyot, M., G., Southworth, S.E. Lindberg, H. Hintelmann, J.D. Lalonde, N. Ogrinc, A.J. Poulain and K.A. Sandilands, 2004. Formation and evasion of dissolved gaseous mercury in large enclosures amended with $^{200}HgCl_2$, *Atmospheric Environment*, 38, 4279-4289.

Bey, I., et al., 2001. Global modeling of tropospheric chemistry with assimilated meteorology: Model description and evaluation, *Journal of Geophysical Research-Atmospheres*, 106, 23,073-23,096.

Duncan, B. N., R.V. Martin, A. Staudt, R. Yevich, and J.A. Logan, 2003. Interannual and seasonal variability of biomass burning emissions constrained by satellite observations, *Journal of Geophysical Research-Atmospheres*, 108, 4040, doi:10.129/2002JD002378.

Hintelmann, H., R. Harris, A. Heyes, J. Hurley, C. Kelly, D. Krabbenhoft, S. Lindberg, J.W.M. Rudd, K. Scott and V. St. Louis, 2002. Reactivity and mobility of new and old mercury deposition in a boreal forest ecosystem during the first year of the METAALICUS study, *Environmental Science and Technology*, 36, 5034-5040.

Holmes, C. D., D. J. Jacob, and X. Yang, 2006. Global lifetime of elemental mercury against oxidation by atomic bromine in the free troposphere. *Geophysical Research Letters*, 33, L20808, doi:10.1029/2006GL027176.

Jaffe, D., E. Prestbo, P. Swartzendruber, P. Weiss-Penzias, S. Kato, A. Takami, S. Hatakeyama, and Y. Kajii, 2005. Export of atmospheric mercury from Asia, *Atmospheric Environment*, 39, 3029-3038.

Pacyna, E.G., J.M. Pacyna, F. Streenhuisen, and S. Wilson, 2006. Global anthropogenic mercury emission inventory for 2000. *Atmospheric Environment*, 40, 4038-4063.

Ryaboshapko, A., et al., 2002. Comparison of mercury chemistry models. *Atmospheric Environment*, 36, 3881-3898.

Selin, N.E., D.J. Jacob, R.J. Park, R.M. Yantosca, S. Strode, L. Jaeglé and D. Jaffe, 2007. Chemical cycling and deposition of atmospheric mercury: Global constraints from observations. *Journal of Geophysical Research-Atmospheres*, 112, D02308, doi:10.1029/ 2006JD007450.

Selin, D.J. Jacob, R.M. Yantosca, S. Strode, L. Jaeglé, and E.M. Sunderland, 2008. Global 3-D land-ocean-atmosphere model for mercury: Present-day versus preindustrial cycles and anthropogenic enrichment factors for deposition. Global Biogeochemical Cycles, doi:10.1029/2007GB003040.

Selin, N.E., and D.J. Jacob, 2008. Seasonal and spatial patterns of mercury wet deposition in the United States: Constraints on the contribution from North American anthropogenic sources. Atmospheric Environment, doi:10.1016/j.atmosenv.2008.02.069

Stohl, A., et al., 2002. On the pathways and timescales of intercontinental air pollution transport. *Journal of Geophysical Research-Atmospheres*, 107(D23), 4684, doi:10.1029/ 2001JD001396.

Strode, S., L. Jaeglé, N.E. Selin, D.J. Jacob, R.J. Park, R.M. Yantosca, R.P. Mason, and F. Slemr, 2007. Air-Sea Exchange in the Global Mercury Cycle. *Global Biogeochemical Cycles*, 21, GB1017, doi:10.1029/2006GB002766.

Strode, S., L. Jaeglé, D.A. Jaffe, P.C. Swartzendruber, N.E. Selin, C. Holmes, and R.M. Yantosca, 2008. Trans-Pacific transport of mercury. Journal of Geophysical Research-Atmospheres, doi:10.1029/2007JD009428.

Swartzendruber, P., D.A. Jaffe, E.M. Presbo, P. Weiss-Penzias, N.E. Selin, R. Park, D.J. Jacob, S. Strode, and L. Jaeglé, 2006. Observations of reactive gaseous mercury in the free troposphere at the Mount Bachelor Observatory. *Journal of Geophysical Research-Atmospheres*, 111, D24301, doi:10.1029/2006JD007415.

Travnikov, O., 2005. Contribution of the intercontinental atmospheric transport to mercury pollution in the Northern Hemisphere. *Atmospheric Environment*, 39, 7541-7548.